Weierstraß-Institut
für Angewandte Analysis und Stochastik

im Forschungsverbund Berlin e.V.

Preprint ISSN 0946 – 8633

Bifurcations in a model of monolithic passively mode-locked semiconductor laser

Andrei Vladimirov [1], Alexander Pimenov [2], Dmitry Rachinskii [2]

submitted: 6th November 2009

[1] Weierstrass Institute for Applied Analysis and Stochastics,
Mohrenstrasse 39,
D - 10117 Berlin,
Germany
E-Mail: vladimir@wias-berlin.de

[2] Dept. of Applied Mathematics
University College Cork
Ireland

E-mail: d.rachinskii@ucc.ie

No. 1458
Berlin 2009

2000 *Mathematics Subject Classification.* 78A60,34C23.

Key words and phrases. semiconductor laser, quantum dots, bifurcations, mode-locking.

1999 *Physics and Astronomy Classification Scheme.* 42.60.Fc 42.55.Px 42.60.Mi 42.65.Pc.

Edited by
Weierstraß-Institut für Angewandte Analysis und Stochastik (WIAS)
Mohrenstraße 39
10117 Berlin
Germany

Fax: + 49 30 2044975
E-Mail: preprint@wias-berlin.de
World Wide Web: http://www.wias-berlin.de/

Abstract

Operation regimes of a two section monolithic quantum dot mode-locked laser are studied theoretically using a model that takes into account carrier exchange between quantum dots and wetting layer. It is shown that when the absorber section length is large enough the laser exhibits bistability between laser off state and different mode-locking regimes. Q-switching instability leading to slow modulation of the mode-locked pulse peak intensity is completely eliminated in this case.

1 Introduction

Mode-locking in lasers is a powerful tool for generating short optical pulses for different practical applications ranging from high speed communications to medical diagnostics. In particular, monolithic passively mode-locked semiconductor lasers are compact sources of picosecond pulses with high repetition rates suitable for applications in telecommunication technology [1, 2]. Recently a new generation of mode-locked semiconductor lasers based on quantum-dot (QD) materials was developed [3]. These lasers demonstrate many advantages over conventional quantum well lasers, such as low threshold current, small alpha factor, low pulse chirp, high stability to noise and external feedback, etc. [4, 5]. It was recently shown that QD mode-locked lasers can generate very short subpicosecond optical pulses [6].

Due to the discrete nature of electron density states in QD lasers, they demonstrate a number of characteristic features distinguishing them from conventional semiconductor devices [7]. Therefore, theoretical modeling of these lasers requires a development of more sophisticated models which would take into account these features. In particular, carrier dynamics in quantum dot lasers includes carrier exchange processes between wetting layer and discrete levels in quantum dots. These processes are characterized by a large number of quite different characteristic time scales, which have an important impact on the quality of mode-locked pulses and the dynamical behavior of the laser in general.

Rate equations describing the carrier exchange dynamics in QD lasers were proposed in [8, 9]. These equations govern the time evolution of three quantities: carrier density in the wetting layer and occupation probabilities of two discrete levels in quantum dots corresponding to the first excited state and the ground state, respectively. Assuming that the carrier relaxation rate from the excited states to the ground state is sufficiently fast one gets only two carrier equations for occupation probability of the quantum dot ground state ρ and carrier density in the wetting

layer n [10, 11]. Similar pairs of carrier rate equations for gain and absorber sections were recently incorporated into the delay differential mode-locking model to describe passive mode-locking in quantum dot lasers [12, 13]. It was shown that fast carrier capturing from the wetting layer to quantum dots can lead to suppression of undesirable Q-switching instability of the fundamental mode-locking regime [11]. Such instability leading to a degradation of the quality of mode-locking regime is quite difficult to eliminate in quantum well mode-locked devices [2, 14]. In this paper, using the delay differential equations (DDE) model and the traveling wave equations, we perform a more systematic study of the effect of carrier exchange processes on the dynamics of a quantum dot mode-locked laser. We show that taking into consideration Pauli blocking terms in carrier exchange equations can lead to a qualitative change in the laser dynamical behavior. When the absorber section length becomes large enough Q-switching instability of fundamental mode-locking regime disappears and a bistability develops between the laser off state and different mode-locking regimes. We also describe the period doubling bifurcation leading to a harmonic mode-locking regime with two different pulses circulating in the cavity.

2 Model equations

We consider a model of passively mode-locked quantum-dot laser consisting of two sections, a forward biased amplifying section and a reversely biased saturable absorber section. In each section the spatial-temporal evolution of the amplitudes of two counter-propagating waves $E^{\pm}$ can be described by the so-called traveling wave equations [15]:

$$\frac{\partial E^{\pm}}{dt} \pm \frac{\partial E^{\pm}}{\partial z} = -\frac{\beta_{g,q}}{2} E^{\pm} + \frac{1 - i\alpha_{g,q}}{2} g_{g,q}(2\rho - 1)E^{\pm}, \tag{1}$$

where the index g corresponds to the amplifying section and the index q refers to the absorber section. The parameters $\beta_{g,q}$ describe linear internal losses in the semiconductor medium, $\alpha_{g,q}$ are the linewidth enhancement factors, and g_g (g_q) is the differential gain (loss) parameter in the amplifying (absorbing) section. Equations (1) are coupled to the equations governing the evolution of the occupation probability of the ground state in quantum dots ρ and the carrier density in the wetting layer n:

$$\frac{\partial \rho}{\partial t} = -\gamma_{g,q}\rho - r_{g,q}\rho + b_{g,q}n(1-\rho) - g_{g,q}(2\rho - 1)\left(|E^{+}|^2 + |E^{-}|^2\right), \tag{2}$$

$$\frac{\partial n}{\partial t} = \eta_{g,q} - \delta_{g,q}n + 2r_{g,q}\rho - 2b_{g,q}n(1-\rho). \tag{3}$$

Here $n = \sigma W$, σ is the wetting layer occupation probability, $W = f/2N^D$, f is the number of states in the wetting layer, and N^D is the total number of quantum dots in the corresponding section. The factor 2 in Eq. (3) accounts for the double degeneracy of the ground state in quantum dots. The parameters $\gamma_{g,q}$ ($\delta_{g,q}$) are the

carrier relaxation rates in wetting layer (quantum dots). The parameters $r_{g,q}$ and $b_{g,q}$ describe, respectively, the rate of carrier escape from quantum dots to wetting layer and carrier capturing rate from wetting layer to quantum dots. Finally, note that in the gain section Eq. (3) contains the term η_g that describes linear gain due to injection current. Since there is no current in the absorber section, we have $\eta_q = 0$. However, we assume that the relaxation time δ_q increases with the increase of the reverse voltage applied to the absorber section. Boundary conditions for Eqs. (1) are given by $E^+(0,t) = \sqrt{\kappa_1}E^-(0,t)$ and $E^-(L,t) = \Gamma\sqrt{\kappa_2}\int e^{-\Gamma\tau}E^+(L,t-\tau)\,d\tau$, where $z = 0$ ($z = L$) corresponds to the left (right) laser facet. These conditions account for the reflectivities of the facets $\kappa_{1,2}$ and the gain dispersion which is described by Lorentzian filter of width Γ [16].

Equations (1)-(3) have been used for numerical modeling dynamics of monolithic quantum dot laser. A numerical scheme for solving these equations is described in [16]. Along with these equations a simplified model assuming ring cavity geometry and unidirectional lasing approximation [12, 13, 17] was used. This model can be written as a set of five delay differential equations [11]

$$\Gamma^{-1}\frac{dA}{dt} + A = \sqrt{\kappa}e^{(1-i\alpha_g)G(t-T)/2+(1-i\alpha_q)Q(t-T)/2}A(t-T), \tag{4}$$

$$\frac{dP_g}{dt} = -\left(\gamma_g + r_g\right)P_g + b_g N_g\left(1-P_g\right) - e^Q(e^G-1)|A|^2, \tag{5}$$

$$\frac{dP_q}{dt} = -\left(\gamma_q + r_q\right)P_q + b_q N_q\left(1-P_q\right) - s(e^Q-1)|A|^2, \tag{6}$$

$$\frac{dN_g}{dt} = \delta_g\left(g_0 - N_g\right) + 2r_g P_g - 2b_g N_g\left(1-P_g\right), \tag{7}$$

$$\frac{dN_q}{dt} = -\delta_q N_q + 2r_q P_q - 2b_q N_q\left(1-P_q\right). \tag{8}$$

Here A is the normalized electric field envelope at the entrance of the absorber section. The variables $P_{g,q} = \int_{g,q}\rho dl/l_{g,q}$ and $N_{g,q} = \int_{g,a} n dl/l_{g,q}$ are normalized integrals of the occupation probability ρ and carrier density n along the the corresponding section where l_g (l_q) denotes the length of the gain (absorber) section. Cumulative saturable gain G and loss Q introduced by the gain and absorber sections are given by

$$G = g_g l_g\left(2P_g - 1\right), \quad Q = g_q l_q\left(2P_q - 1\right).$$

The parameter T is the cavity round trip time, Γ is the spectral filtering width, κ is the attenuation factor that accounts for the linear nonresonant losses $\beta_{g,q}$ and reflectivities of the laser facets $\kappa_{1,2}$. Finally, $g_0 = \int_g \eta_g dl/l_g$ is the linear gain parameter.

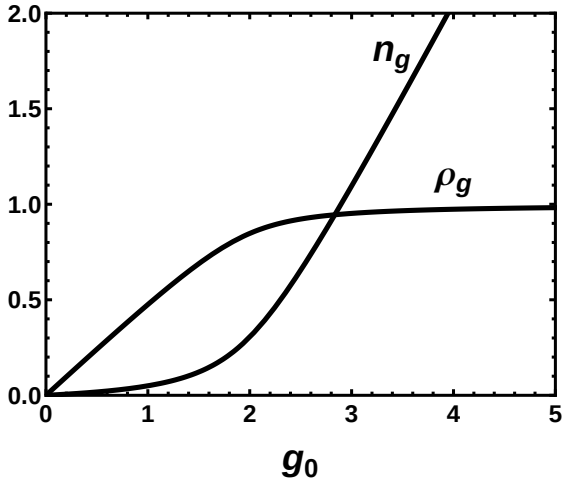

Figure 1: Dependence of the carrier density in wetting layer N_g and occupation probability in quantum dots P_g in the gain section on the linear gain parameter g_0 for the solution with zero laser intensity.

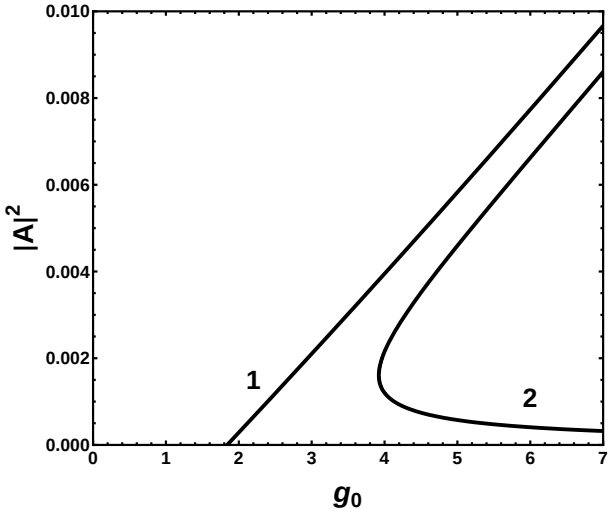

Figure 2: Dependence of the laser intensity on the linear gain parameter g_0. 1 – monostable behavior, short absorber section $l_g = 0.9$ mm, $l_q = 0.1$ mm. 2 – bistable behavior: longer absorber section, $l_g = 0.8$ mm, $l_q = 0.2$ mm. Other parameters are $T = 25$ ps, $\alpha_g = \alpha_q = 0$, $s = 15$, $\Gamma^{-1} = 0.4$ ps, $\kappa = 0.3$, $\gamma_g^{-1} = 1$ ns, $\gamma_q^{-1} = 1$ ns, $\delta_g^{-1} = 1$ ns, $\delta_q^{-1} = 10$ ps, $g_g = 4$ mm^{-1}, $g_q = 10$ mm^{-1}, $b_g^{-1} = 5$ ps, $b_q^{-1} = 5$ ps, $r_g^{-1} = 100$ ps, $r_q^{-1} = 10$ ps.

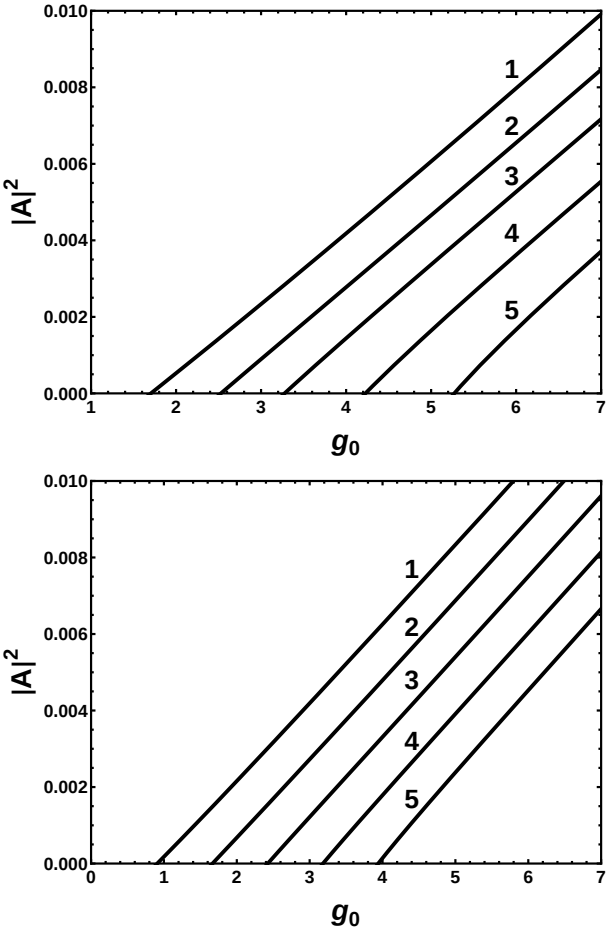

Figure 3: Dependence of cw laser intensity on the gain parameter g_0 calculated for different values of the capturing rate b_g and the relaxation rate γ_g in the gain section. Top: The curves 1, 2, 3, 4, and 5 correspond to $b_g^{-1} = 2$ ps, $b_g^{-1} = 20$ ps, $b_g^{-1} = 36$ ps, $b_g^{-1} = 57$ ps, and $b_g^{-1} = 80$ ps, respectively. Bottom: The curves 1, 2, 3, 4, and 5 correspond to $\gamma_g^{-1} = 200$ ps, $\gamma_g^{-1} = 100$ ps, $\gamma_g^{-1} = 67$ ps, $\gamma_g^{-1} = 50$ ps, and $\gamma_g^{-1} = 40$ ps. Other parameters are the same as in Fig. 2.

3 CW regimes

In this section we study the solutions of Eqs. (4)-(8) corresponding to cw laser output. The simplest cw solution is that corresponding to zero laser intensity. It is given by

$$A = 0,\ P_g = P_{g0},\ N_g = N_{g0},\ P_q = N_q = 0 \tag{9}$$

with

$$P_{g0} = \frac{1+\xi}{2} - \sqrt{\left(\frac{1+\xi}{2}\right)^2 - \frac{g_0\zeta}{2}}, \quad N_{g0} = g_0 - \frac{2P_{g0}}{\zeta}, \tag{10}$$

and

$$\xi = \frac{\zeta}{2}\left(g_0 + \frac{r_g+\gamma_g}{b_g}\right), \quad \zeta = \frac{\delta_g}{\gamma_g}. \tag{11}$$

The dependence of the quantities $P_g = P_{g0}$ and $N_g = N_{g0}$ on the linear gain parameter g_0 in the amplifying section is shown in Fig. 1. We see that unlike the carrier density N_g in the wetting layer, which grows linearly at large linear gains g_0, the growth of the occupation probability P_g of quantum dots saturates at $P_g = 1$ when the injection current becomes sufficiently large. The smaller the ratio $(r_g + \gamma_g)/b_g$ in (11) and the larger ζ, the faster P_g saturates. This saturation is related to the presence of the Pauli blocking factor $1 - P_g$ in the capturing rate term in Eq. (6), hence it is a consequence of the fact that the number of free places for electrons in quantum dots is limited. Saturation of the occupation probability results in saturation of the gain in the amplifying section. This gain can not exceed the maximal value $G = g_g l_g$ corresponding to a state with fully occupied quantum dots, $P_g = \rho_g = 1$.

Since at $A = 0$ the absorber section is completely unsaturated, we have $P_q = 0$ and, hence, the cumulative loss introduced by this section is $Q = -g_q l_q$. Therefore, for $g_0 \to \infty$ when all the states in quantum dots are fully occupied, i.e., $G = g_g l_g$, the stability of the zero intensity cw solution (9)-(11) is determined by the inequality $g_g l_g - g_q l_q + \ln\kappa < 0$, where $\ln\kappa$ describes the linear nonresonant losses. This inequality ensures that the absolute value of the coefficient by the delayed electric field term in Eq. (4) is less than 1. From this condition we see that when the absorber section length is large enough, namely

$$g_q l_q > g_g l_g + \ln\kappa, \tag{12}$$

the zero intensity steady state (9)-(11) remains stable at arbitrary large injection currents (arbitrary large g_0). In this case the maximal achievable linear cumulative gain $G = g_g l_g$ is smaller than total unsaturated losses $|Q| = g_q l_q$ introduced by the absorber section plus linear nonsaturated losses $-\ln\kappa$. However, even in this case laser generation is possible in a regime with strongly saturated absorber. Indeed, considering for simplicity the case of zero linewidth enhancement factors $\alpha_g = \alpha_q = 0$, in the limit $g_0 \to \infty$ one obtains that apart from zero intensity steady state (9)-(11) there exist two cw solutions with $|A|^2 \neq 0$. The first of these cw solutions corresponds to a fully saturated absorber $P_q = 1/2$ and is always stable in this

limit (see the upper branch of curve 2 in Fig. 2). The second solution (the lower branch of curve 2 in Fig. 2) corresponds to the positive occupation probability $P_q = (g_q l_q - g_g l_g - \ln\kappa)/(2g_q l_q) > 0$ only when the inequality (12) is satisfied. Otherwise, this solution corresponds to negative occupation probability and laser intensity, $\rho_q, |A|^2 < 0$, and, therefore, is nonphysical. Thus, if the inequality (12) holds, the branch of nonzero-intensity cw solutions is isolated from the zero intensity state (curve 2 in Fig. 2) and the bistability exists between the two cw states. If the absorber section length is sufficiently short, so that the inequality (12) is not satisfied, the solution with nonzero laser intensity bifurcates from the zero intensity state at gain parameter value

$$g_0 = (g_g l_g + g_q l_q - \ln\kappa)\left[\frac{1}{g_g l_g \zeta} + \frac{r_g + \gamma_g}{b_g\,(g_g l_g - g_q l_q + \ln\kappa)}\right],$$

which corresponds to the linear lasing threshold (see curve 1 in Fig. 2). In this case, either there is no bistability or the bistability domain is rather small.

Fig. 3 illustrates the dependence of the cw solutions of Eqs. (4)-(8) on the parameters of the gain section. According to this figure, both the increase of the capturing rate b_g and the decrease of the relaxation rate γ_g lead to the increase of the cw laser intensity. It should be noted, however, that these plots do not take into account the stability issues.

4 Mode-locking regimes

The results of numerical bifurcation analysis of Eqs. (4)-(8) performed using the path following software package DDEBIFTOOL [18] are summarized in Figs. 4 and 5. These figures show the dependence of the laser field peak intensity on the linear gain parameter g_0 in lasers with two different lengths of the absorber section. Fig. 4 corresponds to a laser with a rather short absorber section when there is no bistability between zero and nonzero intensity cw solutions (see Fig. 2). Bifurcation sequence depicted in this figure is qualitatively similar to that described earlier for a model of a monolithic quantum well mode-locked device [12, 13]. Mode-locking solutions bifurcate from the cw solution corresponding to nonzero laser intensity. At sufficiently small injection currents g_0 the fundamental mode-locking regime exhibits an instability leading to undamped oscillations of the pulse peak intensity at the Q-switching frequency. This instability leads to a regime of "Q-switched" mode-locking, which is indicated *qsml* in Fig. 4 (see also the time trace in Fig. 6b). However, unlike the model of quantum well laser described in [12, 13], the QD mode-locked model (4)-(8) apart from Q-switched mode-locking can exhibit a pure Q-switching regime. This regime, indicated *qs* in Fig. 4, corresponds to a periodic laser intensity (see Fig. 6a for the time trace). With the increase of the injection current Q-switching regime looses stability and a transition to Q-switching mode-locking with quasiperiodic laser intensity takes place. On the contrary, with the increase of the injection current the fundamental mode-locking regime labeled *ml*

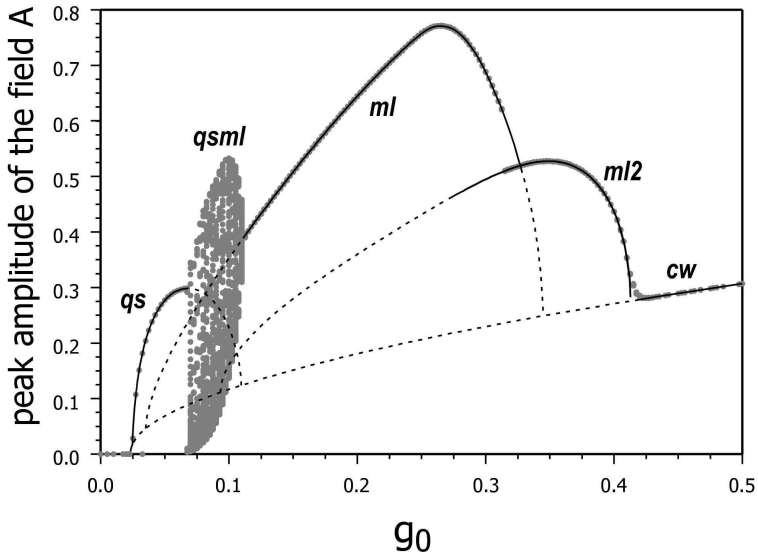

Figure 4: Bifurcation diagram illustrating the sequence of dynamical regimes that takes place with the increase of the linear gain parameter g_0. Solid (dotted) lines correspond to stable (unstable) solutions. Grey dots indicate the extrema of the absolute value of the electric field amplitude $|A|$ obtained by means of direct numerical simulation of Eqs. (4)-(8). *cw*, *ml* , *ml*2, *qs*, and *qsml* correspond to continuous wave, fundamental mode-locking, harmonic mode-locking, Q-switching, and Q-switched mode-locking regimes, respectively. $l_g = 0.9$ mm, $l_q = 0.1$ mm, $g_g = 4$ mm^{-1}, $g_q = 20$ mm^{-1}, $\gamma_n^{-1} = 5$ ps, $b_g^{-1} = 5$ ps, $b_q^{-1} = 5$ ps, $r_g^{-1} = 250$ ps, $r_q^{-1} = 6.67$ ps. Other parameters are the same as for Fig. 2.

becomes stable (see Fig. 6c). This regime is characterized by a sequence of short pulses with the repetition period close to the cavity round trip time. At even larger values of g_0 a transition to harmonic mode locking regime with approximately twice higher repetition rate and finally to a stable cw regime takes place. These regimes are labeled *ml*2 and *cw* in Fig. 4. The time trace corresponding to the regime *ml*2 is shown in Fig. 6d.

Figure 5 presents a diagram similar to that of Fig. 4, but corresponds to a longer absorber section. As it is seen, in this case a bistability appears between zero intensity state and different mode-locked regimes. The branch of fundamental mode-locking regime in Fig. 5 becomes semi-infinite and bistable with the laser-off state. Furthermore, the Q-switching instability of the fundamental mode-locking regime does not appear any more. Thus, by increasing the absorber section length the Q-switching instability can be completely eliminated.

Figure 5 demonstrates another peculiar feature of Eqs. (4)-(8) describing a mode-locked QD laser. For certain parameter values these equations can exhibit a period-doubling bifurcation of the harmonic mode-locked solution with the pulse repetition rate twice larger than that of the fundamental regime. After this bifurcation of the mode-locking regime with two pulses circulating in the cavity, the pulses acquire

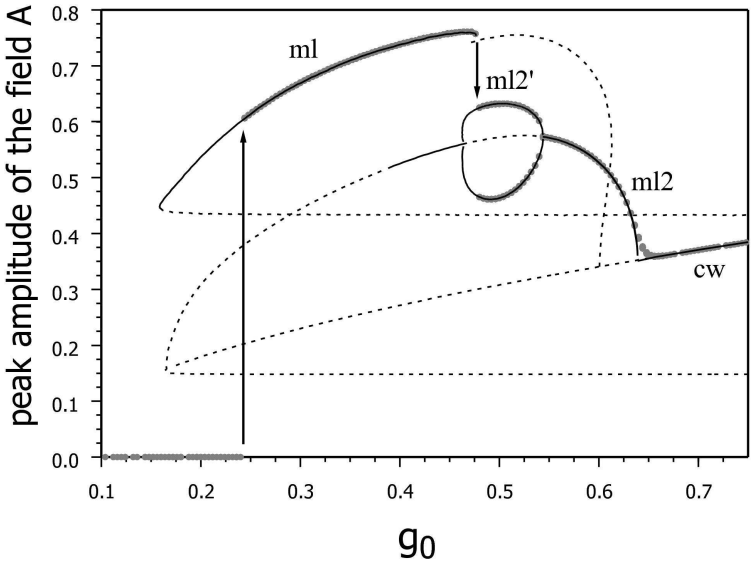

Figure 5: Same diagram as in Fig. 4 but calculated for twice longer absorber section. $\Gamma^{-1} = 0.5$ ps, $l_g = 0.8$ mm, $l_q = 0.2$ mm, $g_g = 2.22$ mm^{-1}, $g_q = 20$ mm^{-1}, $\delta_q^{-1} = 10$ ps, $b_g^{-1} = 1$ ps, $b_q^{-1} = 20$ ps, $r_g^{-1} = 1$ ns, $r_q^{-1} = 10$ ps. Other parameters are the same as for Fig. 2. Arrows indicate jumps between different regimes.

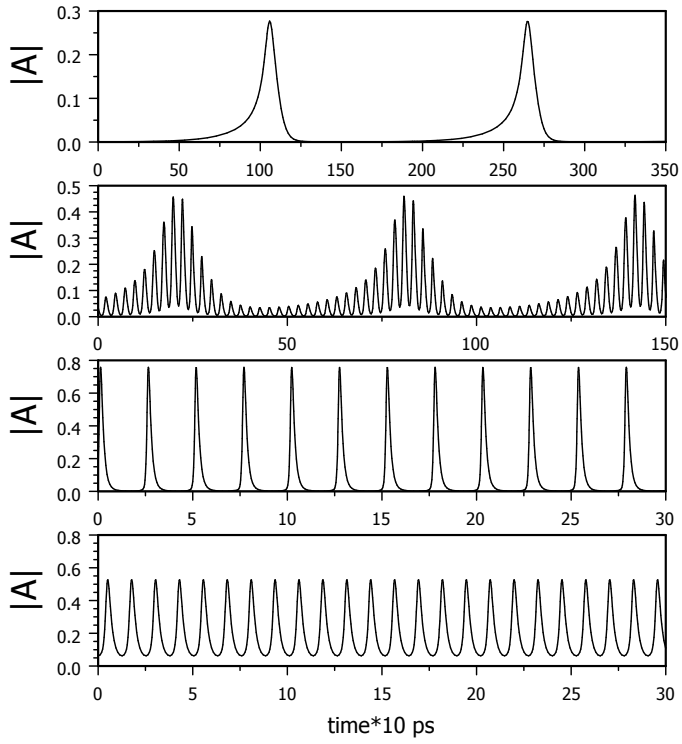

Figure 6: Time traces illustrating different dynamical regimes shown in Fig. 4. (a) – Q-switching (qs); (b) – Q-switched mode-locking ($qsml$); (c) – fundamental mode-locking (ml); (d) – harmonic mode-locking ($ml2$).

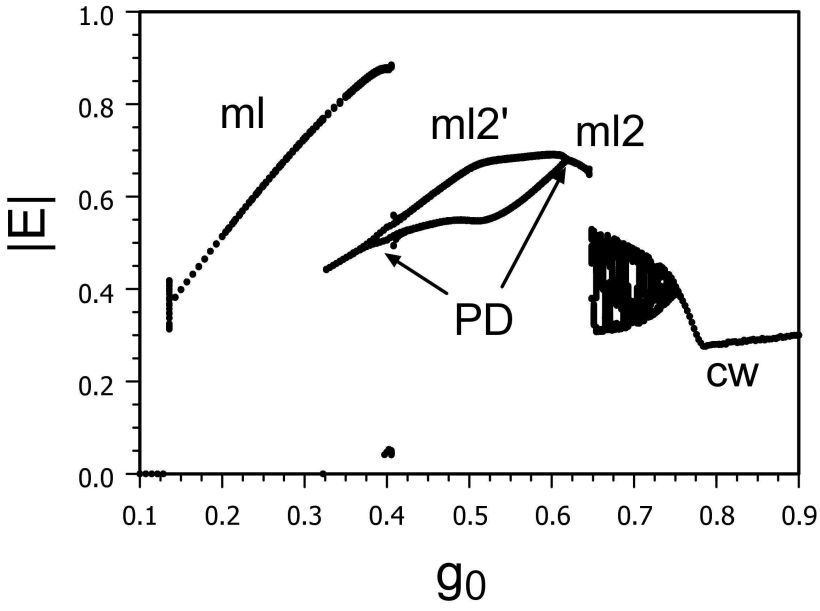

Figure 7: Bifurcation tree obtained from numerical simulations of Eqs. (1)-(3). Black dots correspond to maxima of intensity time traces calculated at different values of the linear gain parameter $g_0 = \eta_g l_g$. Period doubling bifurcations of the harmonic mode-locking regime are labeled PD. $l_g = 1.125$ mm, $l_q = 0.125$ mm, $\Gamma^{-1} = 0.25$ ps, $\kappa_{1,2} = 0.55$, $\beta_g = \beta_q = 0$, $g_g = 2$ mm^{-1}, $g_q = 9$ mm^{-1}, $r_g^{-1} = 20$ ps, $r_q^{-1} = 1$ ns, $\gamma_g^{-1} = \gamma_q^{-1} = 10$ ps, $\delta_g^{-1} = 10$ ps, $\delta_q^{-1} = 1$ ns.

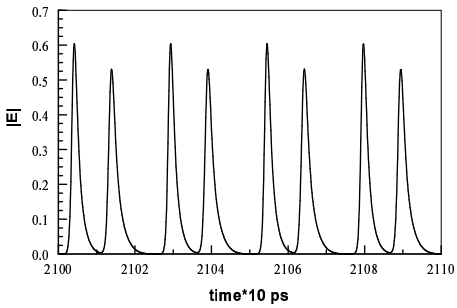

Figure 8: Harmonic mode-locking regime with two pulses having different peak intensities and separations, $g_0 = \eta_g l_g = 0.5$. Other parameters are the same as for Fig. 7.

different amplitudes and separations. This regime is indicated $ml2'$ in Fig. 5. Similar period-doubling bifurcation was found in numerical simulations of the traveling wave equations (1)-(3), see the bifurcation diagram in Fig. 7, which is qualitatively very similar to that in Fig. 5, and time trace in Fig. 8. A regime with two different pulses existing in the cavity simultaneously was recently observed experimentally in a two-section mode-locked QD laser [19]. The period doubling bifurcation shown in Figs. 5 and 7 is different from that described in Ref. [16]. The latter bifurcation is possible only in the case of the linear cavity geometry when an additional passive section is present in the laser cavity. This contrasts to the period doubling bifurcation shown in Fig. 5, which appears in the DDE model of a two section laser assuming the ring laser cavity. This bifurcation is related to the carrier exchange processes.

Two-parameter plots illustrating the dependence of the mode-locking range on the capture and escape rates in the gain and absorber sections are presented in Figs. 9 and 10. They have been obtained by direct numerical simulation of Eqs. (4)-(8). In these figures different dynamical regimes are indicated by different levels of grey color. As we see from the upper panel of Fig. 9, the range of stable fundamental mode-locking (shown by dark grey color) increases with the capturing rate b_g in the gain section. However, this dependence is quite weak: the ordinate axis in this figure uses logarithmic scale. The dependence of mode-locking range on the escape rate r_g in the gain section is, on the contrary, quite strong. As it is seen from the lower panel of Fig. 9, the laser can exhibit stable mode-locking only if the carrier escape rate from quantum dots to the wetting layer is sufficiently small. With the increase of this rate mode-locking regime is replaced by either a cw or a Q-switching behavior. Figure 10 illustrates the dependence of the mode-locking range on the capture and escape rates in the absorber section. According to this figure the range of fundamental and harmonic mode-locking regimes increases with the decrease of the capturing rate b_q and increases with the escape rate r_q. The increase of the mode-locking range is usually accompanied by the appearance of harmonic mode-locking with the pulse repetition rate close to twice the cavity round trip time. However, as it is seen from the lower panel of Fig. 10, when the escape rate r_q to the wetting layer becomes significantly larger then the wetting layer relaxation rate δ_q the mode-locking range starts to decrease with r_q. Speaking more generally, stable mode-locking is possible only if the relaxation rate δ_q and the escape rate r_q are large enough, i.e., the quantum dot absorber is sufficiently fast. This is in agreement with classical results of the mode-locking theory.

Fig. 11 illustrates the influence of the dependence of the mode-locking range on the relaxation rate of the wetting layer. The result here is very similar to that obtained in the quantum well laser [13]. The mode-locking domain increases with the absorber relaxation rate and harmonic mode-locking regimes appear.

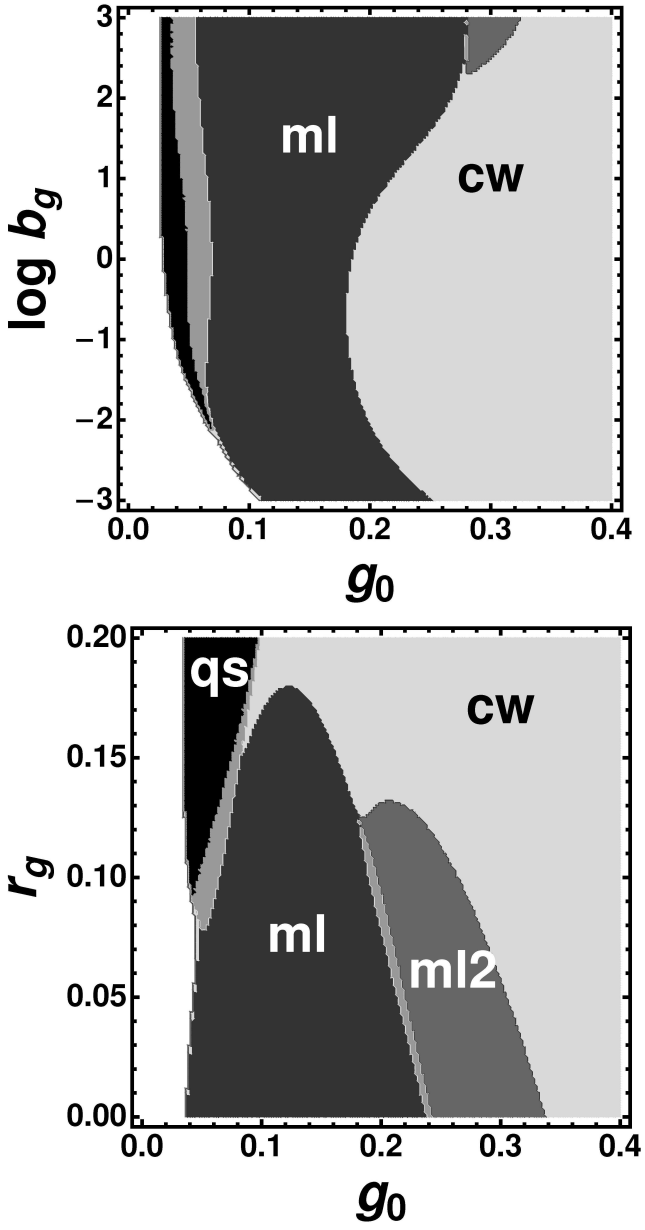

Figure 9: Two parameter diagrams illustrating dependence of mode-locking range on the carrier exchange rates b_g and r_g in the gain section. Different dynamical regimes are indicated by different levels of grey color. White, light grey, grey, dark grey, and black areas indicate, respectively, laser off, continuous wave (cw), fundamental mode-locking (ml), harmonic mode-locking ($ml2$), and Q-switching (qs) regimes. Grey area between fundamental mode-locking and Q-switching domains corresponds to Q-switched mode-locking regime ($qsml$). $s = 15$, $\gamma_q^{-1} = 10$ ps. Upper (lower) panel corresponds to $r_g^{-1} = 250$ ps and $r_q^{-1} = 5$ ps ($b_g^{-1} = 5$ ps and $r_q^{-1} = 2.5$ ps). Other parameters are the same as in Fig. 2.

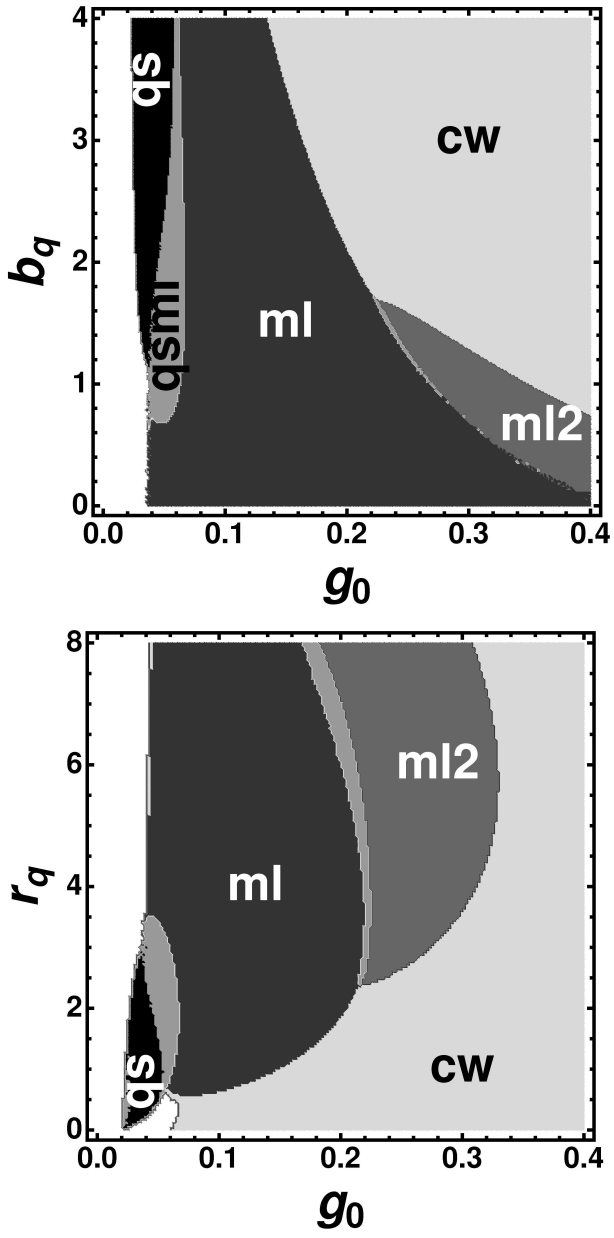

Figure 10: Two parameter diagrams illustrating dependence of mode-locking range on the carrier exchange rates b_q and r_q in the absorber section. Notations are the same as in Fig. 9: ml – fundamental mode-locking regime; ml2 – harmonic mode-locking with approximately twice higher repetition rate; *qs* – Q-switching; *qsml* – Q-switched mode-locking; *cw* – continuous wave regime. $b_g^{-1} = 5$ ps, $r_g^{-1} = 250$ ps. Upper (lower) panel corresponds to $r_q^{-1} = 5$ ps ($b_q^{-1} = 5$ ps). Other parameters are the same as in Fig. 9.

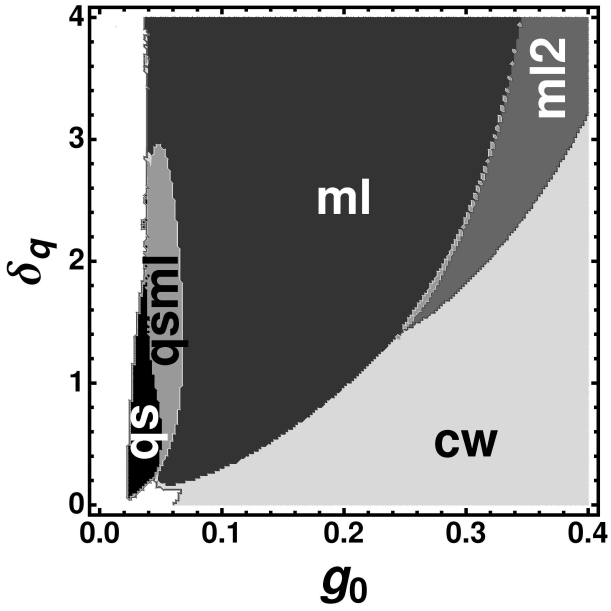

Figure 11: Dependence of the mode-locking range on the absorber relaxation rate δ_q. Notations are similar to those of Fig. 9: ml – fundamental mode-locking regime; $ml2$ – harmonic mode-locking with approximately twice higher repetition rate; qs – Q-switching; $qsml$ – Q-switched mode-locking; cw – continuous wave regime. Parameters are the same as in Fig. 10.

5 Conclusion

To conclude, we have studied the effect of carrier exchange processes between quantum dots and wetting layer on the dynamical behavior of a monolithic mode-locked QD laser. We have presented bifurcation analysis of the set of delay differential equations governing the time evolution of the electric field envelope, occupation probabilities of the ground state in quantum dots, and carrier densities in the wetting layer. In particular, these equations contain Pauli blocking terms which lead to a decrease of the capturing rate when the occupation probability of the ground state in quantum dots increases. We have shown that the dynamical behavior of the laser depends strongly on the relative length of the gain and absorber sections. When the length of the absorber section is relatively small the qualitative behavior of the laser is quite similar to that of the quantum well mode-locking laser model reported in [12, 13, 17]. However when the absorber becomes sufficiently long a bistability appears between zero intensity state and mode-locking regimes. In this case, the Q-switching behavior disappears completely. Another peculiar feature of the QD laser models (4)-(8) is the existence of period-doubling bifurcation of the harmonic mode-locking regime with the repetition frequency approximately twice higher than that of the fundamental mode-locking regime. As a results of this bifurcation a regime with two pulses having different amplitudes and separations in time develops. A similar regime was observed experimentally in a 40 HGz monolithic QD

mode-locked laser [19].

6 Acknowledgments

A. G. V. acknowledges the funding of this work by the SFB787 of the DFG. D. R. was partially supported by the Federal Programme 'Scientists of Innovative Russia', grant 2009-1.5-507-007.

References

[1] L. A. Jiang, E. P. Ippen, and H. Yokoyama, *Ultrahigh-Speed Optical Transmission Technology* (Springer, 2007), chap. Semiconductor mode-locked lasers as pulse sources for high bit rate data transmission, pp. 21–51.

[2] B. Hüettl, R. Kaiser, C. Kindel, S. Fidorra, W. Rehbein, H. Stolpe, G. Sahin, U. Bandelow, M. Radziunas, A.G.Vladimirov, et al., Appl. Phys. Lett. **88**, 221104 (3 pages) (2006).

[3] E. U. Rafailov, M. a. Cataluna, and W. Sibbett, Nature Photonics **1**, 395 (2007).

[4] Kuntz, G. Fiol, M. Lämmlin, D. Bimberg, M. G. Thompson, K. T. Tan, C. Marinelli, R. V. Penty, I. H. White, V. M. Ustinov, et al., Appl. Phys. Lett. **85**, 843 (2004).

[5] L. Shi, Y. H. Chen, B. Xu, Z. C. Wang, Y. H. Jiao, and Z. G. Wang, J. Phys. D: Appl. Phys. **2007**, R307 (40).

[6] E.U.Rafailov, M.A.Cataluna, W.Sibbett, N. Il'inskaya, Yu.M.Zadiranov, A.E.Zhukov, V.M.Ustinov, D. Livshits, A.R.Kovsh, and N.N.Ledentsov, Appl. Phys. Lett. **30**, 081107 (2005).

[7] V. M. Ustinov, A. E. Zhukov, A. Y. Egorov, and N. A. Maleev, *Quantum Dot Lasers* (Oxford University Press, 2003).

[8] A. Markus, J. X. Chen, O. Gauthier-Lafaye, J.-G. Provost, C. Paranthën, and A. Fiore, IEEE J. Sel. Top. Quant. Electron. **9**, 1308 (2003).

[9] A. Markus, M. Rossetti, V. Calligari, D. Chek-Al-Kar, J. X. Chen, A. Fiore, and R. Scollo, J. Appl. Phys. **100**, 113104 (2006).

[10] D. O'Brien, S. P. Hegarty, G. Huyet, and A. V. Uskov, Opt. Lett. **29**, 1 (2004).

[11] E. Viktorov, P. Mandel, A.G.Vladimirov, and U. Bandelow, Appl. Phys. Lett. **88**, 201102 (3 pages) (2006).

[12] A. Vladimirov, D. Turaev, and G. Kozyreff, Opt. Lett. **29**, 1221 (2004).

[13] A. Vladimirov and D. Turaev, Phys. Rev. A **72**, 033808 (2005).

[14] D. Rachinskii, A. Vladimirov, U. Bandelow, B. Hüttl, and R. Kaiser, J. Opt. Soc. Am. B **23**, 663 (2006).

[15] U. Bandelow, H. Wenzel, and H.-J. Wünsche, Electron. Lett. **28**, 1324 (1992).

[16] A. G. Vladimirov, A. S. Pimenov, and D. Rachinskii, IEEE Journal of Quantum Electronics **45**, 462 (2009).

[17] A. Vladimirov and D. Turaev, Radiophys. & Quant. Electron. **47**, 857 (2004).

[18] K. Engelborghs, T. Luzyanina, and G. Samaey, Tech. Rep. TW-330, Department of Computer Science, K.U.Leuven, Leuven, Belgium (2001).

[19] E. Viktorov, P. Mandel, M. Kuntz, G. Fiol, D. Bimberg, A. G. Vladimirov, and M. Wolfrum, Appl. Phys. Lett. (2007).